JOURNAL OF MATERIALS SCIENCE 30 (1995) 1059–1064

NMR characterization of injection-moulded alumina green compacts

Part I *Nuclear spin–spin relaxation*

PU SEN WANG, S. G. MALGHAN, S. J. DAPKUNAS
Ceramics Division, Materials Science and Engineering Laboratory, National Institute of Standards and Technology, Gaithersburg, MD 20899, USA

K. F. HENS, R. RAMAN
Department of Engineering Science and Mechanics, Pennsylvania State University, University Park, PA 16802, USA

Development of proton nuclear magnetic resonance (^{1}H NMR) analysis at 400 MHz has been initiated to evaluate the binder in green injection-moulded alumina compacts. The nuclear spin–spin relaxation times, T_2, of protons in the binder components (paraffin wax, polypropylene, and stearic acid) were measured to allow comparison with those in the injection-moulded green compacts. ^{1}H nuclear spin echo signals were observed by a $(\pi/2)$–τ–π–τ–echo pulse sequence. Bloch's equations were used to calculate the spin–spin relaxation times from these echo intensities. The T_2 for paraffin wax and polypropylene were in the 30–33 μs range and their intensity decay behaviours were very similar. However, the T_2 value for stearic acid was found to be only 17 μs and its echo signal intensity decayed more rapidly than those for paraffin wax and polypropylene. Binder content variations in three green compacts moulded from the same nominal blend composition were detected. Analysis of the moulded compacts also showed the presence of a species with a T_2 value near 300 μs. This unexpected species may be the result of reaction during processing or the presence of moisture. The width of r.f. pulses used to measure echoes did not have a significant effect on relaxation times but should be considered in calculation of echo intensities at equilibrium and, hence, binder composition. This technique development is expected to allow analysis of both binder content and distribution in moulded components with application in process models.

1. Introduction

A need exists for fabrication of structural ceramic components of complex shapes and high dimensional accuracy. Injection moulding offers the opportunity to fabricate complex shapes with high dimensional accuracy and reduce expensive machining. Although injection-moulding technology has been well established for the application of organic polymers, scientific information regarding the application to ceramics has been reported in the literature only recently [1–3]. Several factors impact on the reproducibility and cost of structural ceramic components fabricated by injection moulding. These factors range from materials issues, such as powder characteristics [4–6] and the choice of organic binders [7, 8], to technical aspects including mixing of blends [9–12], moulding [13–15], and binders removal [16]. The transformability between mould dimension and product dimension was also a critical parameter in injection moulding of ceramics [17]. With such complex factors involved in the reproducibility of high-performance ceramics fabrication, sophisticated analysis is required for material diagnosis. Nuclear magnetic resonance (NMR) appears to be one of the most versatile techniques suitable for this endeavour.

In the application of solid-state NMR to ceramic components, several issues need to be addressed. In a rigid lattice of a solid, nuclear spin lattice relaxation (longitudinal relaxation) through the crystal lattice may not occur, resulting in a long nuclear–spin relaxation time, T_1. Rather, the nuclear transverse (spin–spin) relaxation may provide a more effective mechanism for non-equilibrium magnetization decay because of shorter relaxation time, T_2 [18]. Hence, nuclear spin–spin relaxation time becomes an interesting parameter for solids. In the case of $T_2 \ll T_1$, as it is in our samples, T_2 represents the charateristic time for excitation energy to move from one part of the spin system to another. Under this condition, energy put into the spin system by means of radio frequency will long remain in the spin system and thus energy diffusion from one region of the spin system to another before dissipation into molecular motion will occur. The T_2 of polypropylene has been extensively studied

0022–2461 © *1995 Chapman & Hall*

[19–24] with both pulsed and continuous wave (CW) NMR. A relationship between T_2 and molecular motion, molecular weight, crystallinity, and thermal history has been observed.

In this study, NMR characterization of injection-moulded alumina green compacts containing a polypropylene base binder was performed. The objective of the first phase was to develop a detailed understanding of the nuclear spin–spin relaxation phenomenon of these green compacts. The objective of a second phase of this research is to develop an NMR imaging technique for internal structural homogeneity and binder distribution based on the T_2 characteristics. This paper reports the results of the first phase: nuclear spin–spin relaxation.

2. Experimental procedure*

2.1. Ceramic green compacts

The feedstock was prepared by mixing Alcoa A17 alumina powder with a binder containing three components: paraffin wax, polypropylene, and stearic acid. The mixture consisted of 65 vol % alumina and 35 vol % binder. The binder constituents were 62 wt % paraffin wax, 33 wt % polypropylene, and 5 wt % stearic acid. All binder components were in powder form and were blended in a high shear rate blender with intensifier bar for 10 min at 60 r.p.m. blending bowl speed and 3000 r.p.m. intensifier bar speed. This powder mixture was fed via a vibratory/screw-type feeder into a twin-screw processor at 27 $cm^3 min^{-1}$.

Injection moulding was performed using a feedback-controlled Engel powder injection-moulding machine. This is a microprocessor-controlled injection-moulding machine specially equipped to process metal and ceramic powders. All parts were processed using the same moulding conditions. A nozzle/barrel temperature profile of 105, 110, 110, 97 °C from nozzle through three barrel heating sections was used. The feeding throat of the moulding machine was chilled to 18 °C. The mould temperature was kept constant via a water circulator at 28 °C. Injection was performed at a fixed, feedback-controlled filling speed profile. During filling of sprue and runner system, a screw speed of 6 $cm s^{-1}$ was used for the 22 mm diameter screw. Once the left-front reached the gate, the speed was reduced to 1 $cm s^{-1}$. This is done to avoid "jetting" of the material through the mould, resulting in back-filling. Subsequently, the speed was increased to 8.4 $cm s^{-1}$ to ensure the entire fracture bar was filled before the material solidified. The entire filling cycle took 0.3 s. Once a piezo-electric quartz cavity pressure transducer sensed 2 MPa in the mould cavity, control was changed over to pressure control for packing. This stage is to compress the feedstock in the cavity to make up for shrinkages during cooling and solidification of the compact. A pressure profile ranging from 20–30 MPa was applied to the melt for 2 s. A 15 s cooling cycle was used before the mould was opened and the compact ejected.

Each of the three green compact samples was approximately 13 mm × 13 mm × 3.2 mm. Each sample was placed into a 20 mm diameter NMR tube individually for T_2 measurements. The amount of paraffin wax, polypropylene, and stearic acid powder used for the background study was measured so that each of their spin echo intensities will be approximately equal to that of a green compact detected at a 6 μs delay time.

2.2. NMR spectrometer and T_2 measurements

The NMR facility consists of a Bruker MSL-400 system with micro-imaging accessories. The T_2 measurements were performed in the radio frequency resonant coils (r.f. coils) of the imaging probe. This spectrometer has a superconducting magnet of 9.394 T which corresponds to a ^1H resonant frequency of ~ 400 MHz. Our actual resonant frequency was 400.159 972 ± 0.000 001 MHz. Usually, a 20 mm r.f. coil was used for the detection of the ^1H nuclear echo signal from the binder. In some cases, a 10 mm coil was used for comparison. The π/2 pulse width was 19.5 μs for the 20 mm coil.

The T_2 was measured by a multiple pulse sequence of $(\pi/2)$–τ–(π)–τ–echo-D_0 to detect the nuclear echo signals. In this sequence, the $(\pi/2)$ is a 90° r.f. pulse that flips the nuclear bulk magnetization vector, M, from the z-axis to the y-axis. The variable delay, τ, ranges from 6–100 μs. The π is a 180° r.f. pulse and its width is 39 μs for the 20 mm coil. D_0 (20 s in our experiments) is a long delay for the nucleus to return to equilibrium by releasing excitation energy through the crystal lattice. A nuclear echo signal will be detected at the end of the second delay, τ, according to Hahn [25, 26]. If we measure the echo signals for a series of delays (τ = 6, 8, 10, 15, 20, 25, 30, 40, 50, 60, 70, 80, 90 and 100 μs), T_2 can be calculated from the change in echo signal intensity. In our experiment, π_y rather than π_x was used for the 180° excitation. Here x and y represent the coordinates along which the excitation was delivered. This approach is similar to the Carr–Purcell/Meiboom–Gill sequence [27, 28].

Samples of paraffin wax, polypropylene, stearic acid and three bars of injection-moulded alumina green compacts were subjected to the measurement of nuclear spin–spin relaxation times in a 20 mm diameter radio frequency (r.f.) resonant coil. The 90° $(\pi/2)$ pulse width was calculated by taking half of the 180° pulse width which showed no free induction decay (FID) signal in a single-pulse programme. The calculated 90° pulse width was further confirmed to have a maximum FID intensity in a single-pulse measurement. The nuclear echo intensities at equilibrium I_0, and T_2's were calculated by a pascal program, named SIMFIT.

* Certain commercial equipment, instrument, or materials are identified in this paper in order to specify adequately the experimental procedure. Such identification does not imply recommendation or endorsement by the National Institute of Standards and Technology, nor does it imply that the materials or equipment identified are necessarily the best available for the purpose.

The resonant probe has a weak proton signal because the materials used to build the probe contain protons. A set of experiments to record the echo signal intensities was performed for various delays and data stored in a computer for background subtraction. Echo signals of the samples were recorded under identical spectrometer parameters with "absolute intensity" setting to one ($AI = 1$) for comparison. Four scans were collected for each echo. The signals were Fourier-transformed, background subtracted, and integrated for intensity.

3. Results and discussion

The nuclear spin–spin relaxation time, T_2, was measured by a multiple pulse sequence of $(\pi/2)_x$–τ–$(\pi)_y$–τ–echo to detect the nuclear echo signals. In this manner, the $(\pi/2)_x$ is a 90° r.f. pulse (19.5 μs pulse width) parallel to the x-axis that flips the nuclear bulk magnetization vector, M, from the z-axis to the y-axis. During the variable delay, τ, the xy component of this bulk nuclear magnetization vector, M_{xy}, starts to fan out and lose phase coherence on the xy plane because of the magnetic field inhomogeneity and the characteristic spin–spin relaxation times of paraffin wax, polypropylene, and stearic acid. The $(\pi)_y$ is a 180° pulse (39 μs pulse width) parallel to the y-axis that rotates the dephased M_{xy} components on the xy plane about the x-axis. A nuclear echo signal will be detected at the end of the second delay, τ. Nuclear echo signal intensities were measured for the delays (τ) of 6, 8, 10, 15, 20, 25, 30, 40, 50, 60, 70, 80, 90 and 100 μs in the $(\pi/2)_x$–τ–$(\pi)_y$–τ–echo–D_0 sequence. The echo intensities detected at these delays are tabulated in Table I for the pure binder components and in Table II for the three injection-moulded alumina green compacts. The masses of the pure component samples are 0.144 89 ± 0.000 01 g, 0.143 12 ± 0.000 01 g, and 0.385 47 ± 0.000 01 g for paraffin wax, polypropylene, and stearic acid, respectively. The parameters of the spectrometer were set in such a way that, at $\tau = 6$ μs, the integrated nuclear spin echo intensity for wax was near 100 for ease of comparison. At this delay, the echo intensities are 91.0, 89.7, and 95.6, in arbitrary units, for wax, polypropylene, and stearic acid, respectively. Adjusting for differences in the sample sizes, the spin echo intensities per gram sample are 628.1, 626.7, and 248.0 for wax, polypropylene, and stearic acid, respectively. Thus, we can conclude that stearic acid is a low echo-intensity compound compared to wax and polypropylene. A plot of the intensity versus delay time in Table I is shown in Fig. 1. This figure shows clearly that the spin echo intensity decay rate of wax is very close to that of the polypropylene. But the nuclear relaxation rate of the stearic acid is quite different from that of the wax or polypropylene – with a much faster decay rate and thus a shorter T_2.

According to Bloch's equations [29]

$$dM_x/dt = \gamma(\boldsymbol{M} \times \boldsymbol{H})_x - M_x/T_2 \quad (1)$$

and

$$dM_y/dt = \gamma(\boldsymbol{M} \times \boldsymbol{H})_y - M_y/T_2 \quad (2)$$

TABLE I ^{1}H spin-echo intensity decay of paraffin wax, polypropylene, and stearic acid

Delay, τ(μs)	Nuclear echo intensity (Arb. units)		
	Wax	Polypropylene	Stearic acid
6	91.0	89.7	95.6
8	77.1	72.9	71.0
10	67.8	62.2	53.3
15	50.5	46.9	32.7
20	36.1	32.6	19.4
25	27.6	26.5	12.9
30	19.5	20.0	9.0
40	9.9	14.0	5.3
50	6.0	9.8	4.5
60	3.4	8.0	4.0
70	2.6	6.7	3.8
80	1.4	5.5	3.7
90	0.92	4.4	3.3
100	0.90	4.2	3.1
Sample weight	0.144 89 ± 0.000 01 g	0.143 12 ± 0.000 01 g	0.385 47 ± 0.000 01 g

TABLE II ^{1}H spin-echo intensity decay of injection-moulded alumina green compacts

Delay, τ(μs)	Nuclear spin-echo intensity (Arb. units)		
	Sample 1	Sample 2	Sample 3
6	100	77.7	90.8
8	89.5	69.9	78.5
10	81.7	64.1	71.9
15	64.8	51.3	56.1
20	52.1	37.9	43.8
25	42.7	29.1	36.0
30	35.8	25.4	29.1
40	27.6	18.9	21.9
50	23.2	15.7	18.6
60	21.1	13.3	15.7
70	19.3	12.3	14.1
80	17.1	10.9	12.7
90	16.3	9.9	12.1
100	15.3	9.4	11.6
Sample weight	1.479 98 ± 0.000 01 g	1.455 01 ± 0.000 01 g	1.577 30 ± 0.000 01 g

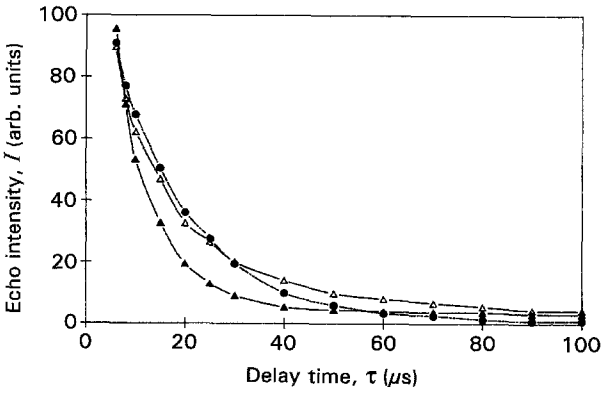

Figure 1 A comparison of integrated ^{1}H spin echo signal intensity versus delay time for (●) paraffin wax, (△) polypropylene, and (▲) stearic acid.

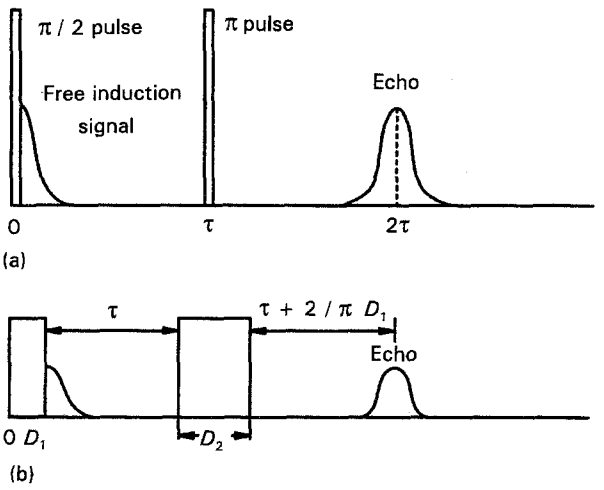

Figure 2 (a) $\pi/2$–τ–π–τ–echo multiple pulse sequence for detection of nuclear echo. The echo will be observed at 2τ when τ is large compared to the r.f. pulse width. (b) When the r.f. pulse width is not small enough to be ignored as compared to τ, the echo will be detected at $2\tau + [3 + (2/\pi)]D_1$, where D_1 is the 90° r.f. pulse width.

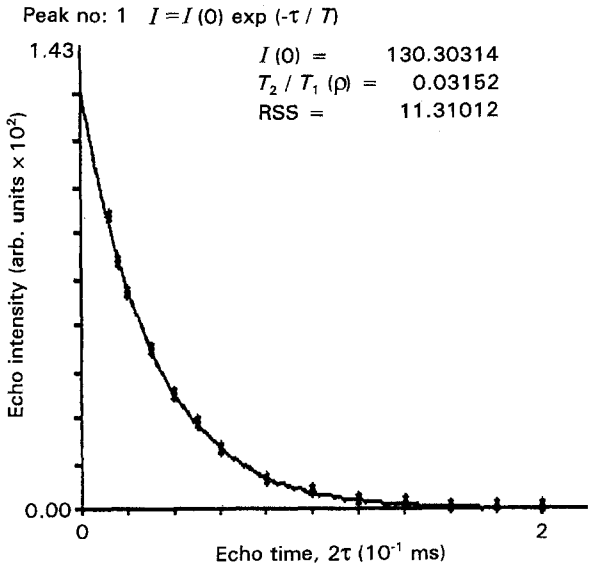

Figure 3 An example of spin echo intensity versus 2τ plot for a wax sample, the data was used to calculate T_2 at 2τ echo time from Equation 3.

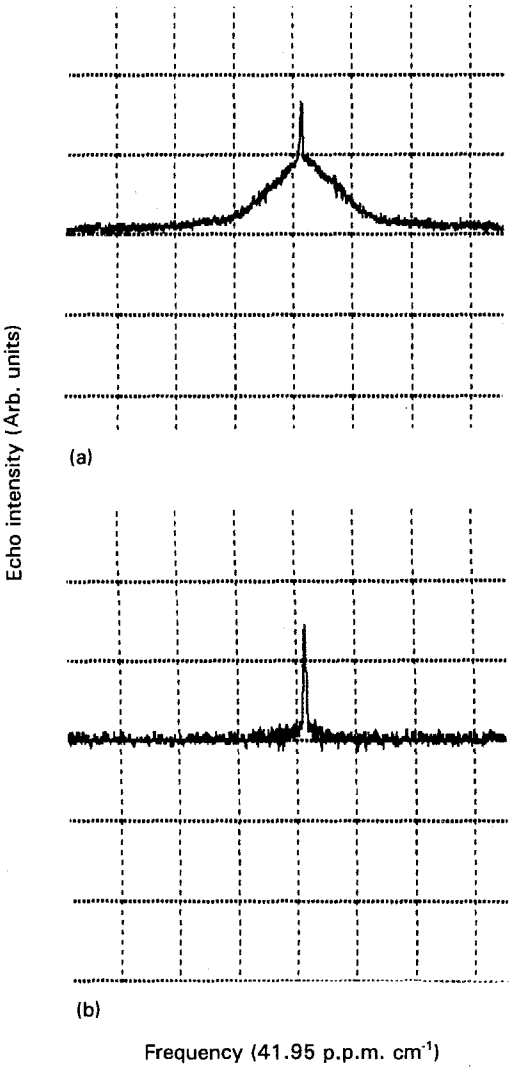

Figure 4 (a) Fourier-transformed nuclear spin echo signal of a stearic acid sample, at $\tau = 8$ μs, shows a narrow peak from mobile protons, probably due to the surface moisture. (b) At $\tau = 70$ μs, the broad signal from stearic acid has almost disappeared, but the narrow line remains, indicating a longer T_2 of the mobile protons.

where **H** is the total magnetic field and γ is the gyromagnetic ratio. The component of the nuclear magnetization vector on the xy plane will decay exponentially via T_2 causing the spin echo intensity observed at time, t, to decrease exponentially according to

$$I = I_0 \exp(-t/T_2) \quad (3)$$

where I_0 is the echo intensity at equilibrium [30]. T_2 can be calculated from Equation 3 using the values of I and τ when the echo occurs at $t = 2\tau$. Fig. 2a is an example of such a multiple pulse sequence. T_2 values of 31.5, 33.5, and 17.7 μs for paraffin wax, polypropylene, and stearic acid, respectively, were obtained by substituting τ and echo intensity values (Table I) into Equation 3. Considering the variability in molecular weight, crystallinity, and thermal history that affect T_2, our measured 33.5 μs agrees well with the published value of polypropylene [19]. Fig. 3 shows I versus 2τ data measured for a wax sample. Using these data in Equation 3 allows calculation of T_2. In addition to a shorter T_2, we have also observed a type of more "mobile" protons in the stearic acid sample. These protons may be due to surface-adsorbed moisture on stearic acid powders. After Fourier transformation, they give a characteristic narrow line on top of the broader line from the solid. Fig. 4a shows such a line at $\tau = 8$ μs. However, because of a much longer T_2 in the mobile protons, the decay rate of stearic acid will not be altered by these mobile protons. Fig. 4b shows, at $\tau = 70$ μs, almost a complete decay of the stearic acid nuclear echo signal while the narrow peak due to the mobile protons remains.

An echo will be detected at 2τ only if the r.f. pulse widths ($\pi/2$ and π) are small compared to the τ. The 20 mm r.f.-coil used in this study has a π-pulse width of 39 μs ($D_1 = 19.5$ μs, $D_2 = 39$ μs where D_1 and D_2 represent the width for 90° and 180° pulse, respectively). The τ we used could be as short as 6 μs. The

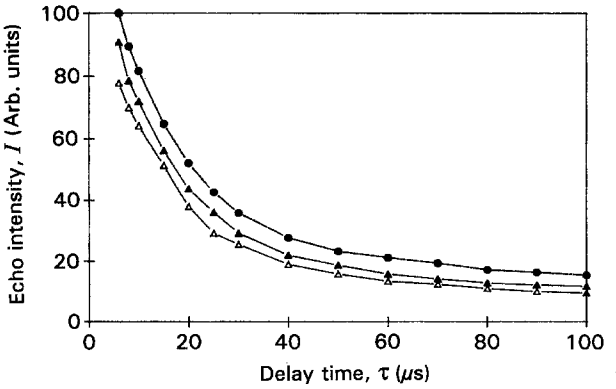

Figure 5 A comparison of integrated ^1H spin echo signal intensity versus delay time for injection-moulded alumina green compacts: (●) Sample 1, (△) Sample 2, (▲) Sample 3.

D_1 and D_2 values, then, cannot be ignored. Fig. 2b shows the actual pulse sequence in our experiment. According to Slichter [30], the time between the end of π-pulse and the peak of the echo signal should be $[\tau + (2/\pi)D_1]$. The echo time, TE, will then be

$$TE = D_1 + \tau + 2D_1 + \tau + (2/\pi)D_1$$
$$= 2\tau + 67.3\ \mu s \quad (4)$$

for $D_1 = 19.5\ \mu s$. The relationship between echo intensity and TE will be

$$I = I_0 \exp(-TE/T_2) \quad (5)$$

The T_2 values did not alter drastically by using Equation 5 for calculation, because they are calculated from the intensity decay rate. We obtain 30.2, 32.1, and 16.4 μs for wax, polypropylene, and stearic acid, respectively. These values are comparable to the values of 31.5, 33.5, and 17.7 μs obtained without considering the π and π/2 pulse widths. It does, though, influence the echo intensity at equilibrium, I_0, because T_2 is calculated based on the rate of decay of the echo intensity, while I_0 is related to the time at which the echo is detected.

Fig. 5 is a plot of the integrated proton echo intensities versus the variable delay times, τ, for the three alumina green compacts. The weight of these compacts were 1.479 98 ± 0.000 01 g, 1.455 01 ± 0.000 01 g, and 1.577 30 ± 0.000 01 g for sample 1, 2, and 3, respectively. The theoretical nuclear spin echo intensity ratio for these three green compacts should be the same as the weight ratio, which is 100.0 : 98.3 : 106.5, if all compositions are the same. We measured an intensity ratio of 100.0 : 77.7 : 90.8 for these samples. It can be concluded, then, that Sample 1 has the highest binder concentration and Sample 2 has the lowest. Another possibility is that Sample 2 contains more stearic acid which exhibits a lower echo intensity per unit weight. A careful examination of the decay behaviour in Fig. 5 does indicate that Sample 2 may have decayed more rapidly than 1 and 3 in the τ = 15–30 μs region.

A comparison of the nuclear echo decay curves of the green compacts in Fig. 5 to those of the pure binder components in Fig. 1 clearly indicates that a species of protons with much longer T_2 values than those of wax, polypropylene, or stearic acid was found in the green compacts. Calculations of T_2 for the mobile species using SIMFIT from Equations 4 and 5 gives T_2 values at 250–300 μs and an intensity of 2%–2.5% of that measured for the green compact. The source of these protons is not clear. They may be from the moisture trapped in the green compacts during injection moulding, evaporated or decomposed from the binder during thermal treatment. Quantification of stearic acid in these green compacts was difficult due to: (1) its low concentration, (2) the high r.f. pulse width to τ ratio causes unreasonable extrapolation to obtain I_0, and (3) the nuclear echo intensity per unit weight from the stearic acid represents only approximately 40% of those from wax or polypropylene.

4. Conclusion

NMR is a versatile technique for ceramic materials characterization. Nuclear spin–spin relaxation time, T_2, is a useful parameter that can be used to study the binder content and composition in ceramic green compacts. Injection-moulded green compacts are suitable candidates for this type of study because of their high binder content and multiple binder component.

The T_2 values for paraffin wax, polypropylene, stearic acid, and injection-moulded alumina green compacts were measured by the $(\pi/2)_x$–τ–π_y–τ–echo–D_0 spin echo at proton frequency in a 9.394 T magnetic field.

Binder content variation in the green compacts, fabricated from the same feedstock, were detected from nuclear spin echo signal intensities. The nuclear spin–spin relaxation times for paraffin wax polypropylene were approximately 30 μs, and their intensity decay behaviours were very similar. However, T_2 of stearic acid was found to be only 17 μs and the echo signal intensity decays more rapidly than that of paraffin wax and polypropylene. The results also indicate that during the process of injection moulding, a new species with T_2 near 300 μs was formed.

The effect of the r.f. pulse width on the relaxation time was found to be insignificant. However, its influence on the calculation of echo intensities at equilibrium, thus the composition of the binder, should be carefully considered.

Acknowledgements

The authors thank Professor R. M. German, Department of Engineering Science and Mechanics, Pennsylvania State University, for his advise and suggestions on injection-moulding technology, and Dr Robert Taylor of Bruker Instruments for interesting discussions on NMR.

References

1. R. M. GERMAN, K. F. HENS and S. T. P. LIN, *Ceram. Bull.* **70** (1991) 1294.
2. M. J. EDIRISINGHE and J. R. G. EVANS, *Int. J. High Technol. Ceram.* **2** (1986) 1.

3. *Idem, ibid.* **2** (1986) 249.
4. J. A. MANGELS and W. TRELA, "Advances in Ceramics", Vol. 9, edited by J. Mangels (American Ceramic Society, Columbus, OH, 1984) p. 220.
5. B. C. MUTSUDDY, *Proc. Br. Ceram. Soc.* **33** (1983) 117.
6. K. H. SWEENEY and R. D. GECKLER, *J. Appl. Phys.* **25** (1954) 1135.
7. A. JOHNSON, E. CARLSTROM, L. HERMANSSON and R. CARLSSON, *Proc. Br. Ceram. Soc.* **33** (1983) 139.
8. A. M. LITMAN, N. R. SCHOTT and S. W. TOZLOWSKI, *Soc. Plas. Eng. Technol.* **22** (1976) 549.
9. F. F. LANGE, *J. Am. Ceram. Soc.* **66** (1983) 393.
10. B. KELLET and F. F. LANGE, *ibid.* **67** (1984) 369.
11. F. F. LANGE and F. METCALF, *ibid.* **66** (1983) 398.
12. F. F. LANGE, B. E. DAVIS and I. A. AKSAY, *ibid.* **66** (1983) 407.
13. I. PELTSMAN and M. PELTSMAN, *Interceram.* **4** (1984) 56.
14. J. A. MANGELS, *Ceram. Eng. Sci. Proc.* **3** (1982) 529.
15. I. I. RUBIN, "Injection Moulding Theory and Practice" (Wiley, New York 1972) pp. 270–317.
16. A. JOHNSSON, E. CARLSTROM, L. HERMANSSON and R. CARLSSON, *Proc. Br. Ceram. Soc.* **33** (1983) 139.
17. K. NAGAYA, A. SOBAJIMA and H. YANO, *Am. Suppl. Inst. J* **4** (1991) 7.
18. D. WOLF, "Spin-Temperature and Nuclear-Spin Relaxation in Matter: Basic Principles and Applications" (Clarendon Press, Oxford, 1979) Ch. 5.
19. H. TANAKA, *Eur. Polym. J.* **21** (1985) 673.
20. M. ITO, H. SERIZAWA, K. TANAKA, W. P. LEUNG and C. L. CHOY, *J. Polym. Sci. Polym. Phys. Edn* **21** (1983) 2299.
21. H. TANAKA, *J. Appl. Polym. Sci.* **27** (1982) 2197.
22. M. P. McDONALD and I. M. WARD, *Proc. Phys. Soc.* **80** (1962) 1249.
23. V. J. McBRIERTY, D. C. DOUGLASS and D. R. FALCONE, *J. Chem. Soc. Faraday Trans. II* **68** (1972) 1051.
24. V. J. McBRIERTY, D. C. DOUGLASS and P. J. BARHAM, *J. Polym. Sci. Polym. Phys. Ed* **18** (1980) 1561.
25. E. L. HAHN, *Phys. Rev.* **80** (1950) 580.
26. W. KUHN, *Angew. Chem.* **29**(1) (1990) 1.
27. H. Y. CARR and E. M. PURCELL, *Phys. Rev.* **94** (1954) 630.
28. S. MEIBOOM and D. GILL, *Rev. Sci. Instrum.* **29** (1958) 6881.
29. F. BLOCH, *Phys. Rev.* **70** (1946) 460.
30. C. P. SLICHTER, "Principles of Magnetic Resonance" (Springer, Berlin, 1989) Ch. 2.

Received 6 May
and accepted 10 December 1993